EUSIPCO 2013 1569743357

ACCURACY LIMITS OF A SEAM-TRACKING ALGORITHM FOR MICROWAVE SYSTEMS AT MM-WAVE FREQUENCIES

Jochen O. Schrattenecker[#], Stefan Schuster[#], Andreas Haderer[#], Guenther Reinthaler[+], and Andreas Stelzer[#]

[#]Institute for Comm. Engineering and RF-Systems, Altenberger Str. 69, A-4040 Linz, Austria
[+]Fronius International GmbH, Guenter Fronius Str. 1, A-4600 Wels-Thalheim, Austria
Email: *j.schrattenecker@nthfs.jku.at*

ABSTRACT

This paper examines a novel concept for estimating the position of a lap joint based on polarimetric scattering effects. While the principle measurement method and setup have already been presented in [1] we focus on the associated accuracy limits, i.e., the Cramér-Rao lower bound (CRLB) calculation for this approach. The minimum achievable position estimation variance is calculated for a variety of estimation scenarios. These calculations are then validated with simulations and real world measurements.

***Index Terms*—** Accuracy, Cramér-Rao bounds, radar polarimetry, radar tracking, millimeter wave radar

1. INTRODUCTION

A novel concept for detecting the exact position of electrically well conductive lap joints by using microwave sensors was introduced in [1, 2]. The basic idea of this concept is to use local polarimetric effects which occur at discontinuities in perfectly conducting surfaces, such as edges, wedges, and steps [3]. The polarized scattering parameters are then used to detect the position of the discontinuity in the surface. Since radar sensors are largely unaffected by environmental stress, this concept is very attractive for automated welding applications. Exact knowledge of the joint's location is important for correct positioning of the welding head and thus also for increasing the quality of the welding process. The best evidence of the capability of a novel sensor system are the accuracy limitations of the measured and estimated parameters when using a specified measurement setup.

Therefore, our goal in this paper is to establish the accuracy limits of the signal processing for detecting the position of a lap joint step by using polarimetric scattering effects. For the measurements and simulations, we used the concept of a frequency-modulated continuous-wave (FMCW) radar [4]. We calculated the best possible performance given by the CRLB, which is asymptotically achieved by estimators derived by means of the maximum likelihood (ML) principle. We focus especially on the influence of step thickness on the position estimation of lap joints. Further, we present a possible signal processing work-flow which practically achieves the CRLB. The results of the CRLB calculations were verified by measurements and Monte Carlo (MC) simulations for different scenarios.

2. MEASUREMENT AND SIMULATION SCENARIO

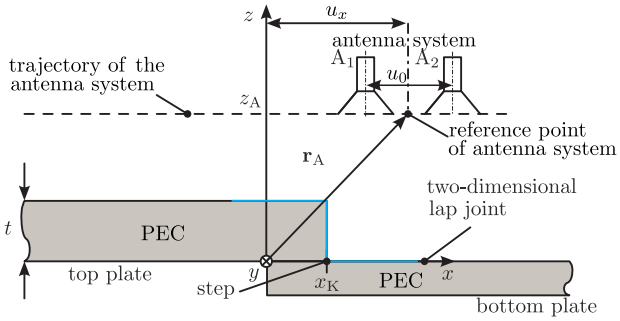

Fig. 1: Schematic diagram showing the target geometry and the antenna system used to describe the simulation model and the measurement setup.

Fig. 1 shows the basic arrangement of a polarimetric synthetic aperture radar (SAR) measurement setup. The configuration serves as a reference for all simulation and measurement scenarios described. The target consists of two metal plates, which are assumed to be perfectly electrically conducting (PEC), arranged in a lap joint geometry.

For the antenna system, two pyramidal horn antennas which radiate a linearly polarized field were selected. Since we are interested in polarimetric effects, the linearly polarized antennas must be mounted in a cross-polarized configuration. This means that the antennas are rotated by $45°$ and $-45°$, respectively, on the rotation axis z. For the scenario it is assumed that the plates of the lap joint are large compared to the antenna footprints in the target plane. Hence, only a single step is illuminated by the antenna system.

The position of the step x_K is to be estimated. To gain cross range resolution, the antenna system is moved along a trajectory in the x-direction parallel to the target plates - a concept known as synthetic aperture [5, 6]. The reference position of the antenna system is described by the vector $\mathbf{r}_A =$

$[u_x, 0, z_\mathrm{A}]^T$, where u_x denotes the radar's location along the one-dimensional aperture and z_A describes the height of the antennas. Further, slant range resolution must be achieved to separate the lap joint from other targets and interferences such as multipath reflections. This is made possible by performing a frequency sweep with the radar hardware, according to the FMCW principle. The properties of the antenna system, the FMCW radar, and the SAR parameters are listed in Tab. 1. For the measurements the radar is moved to a position along the synthetic aperture. Subsequently, a frequency sweep is performed, measurements are taken, and then the radar is repositioned and the process repeated. A two-dimensional intermediate frequency signal

$$s_{\mathrm{IF},12}(k_\mathrm{r}, u_x) = A_\mathrm{IF} W_\mathrm{IF}(k_\mathrm{r}, u_x) e^{-\mathrm{j}2k_\mathrm{r}R} \\ e^{-\mathrm{j}\phi_\mathrm{IF}} \; S_{12}(u_x)|_{k_c} \tag{1}$$

is obtained by the radar system. The signal depends on the position of the antennas u_x and the wavenumber $k_\mathrm{r} = \frac{2\pi k_\mathrm{f} t}{c_0}$, where k_f specifies the slope of the linearly increasing frequency ramp and c_0 stands for the propagation velocity of the electromagnetic wave. The time sampling of (1) yields $t = nT_\mathrm{s}$ with the sampling interval T_s and the sampling index $n = 0 \ldots N-1$, where N is the number of sampling points. The variable $A_\mathrm{IF} e^{-\mathrm{j}\phi_\mathrm{IF}}$ refers to the complex amplitude of the target positioned at R, and $W_\mathrm{IF}(k_\mathrm{r}, u_x)$ denotes the radiation characteristic of a bistatic cross-polarized measurement. The remaining part $S_{12}(u_x)|_{k_c}$ accounts for an amplitude variation based on the radiation characteristic and the target's shape and a phase variation based on the target's position, at the center frequency k_c. This term is particularly important for future signal processing tasks.

Table 1: Measurement setup, FMCW, and SAR parameters

Antenna system		
Antenna gain	G	$\approx 20\,\mathrm{dBi}$
Position of the antenna system	$\mathbf{r}_\mathrm{A}$	$[u_x, 0, 0.15]^T$ m
Polarization angle antenna 1	φ_{A_1}	$45°$
Polarization angle antenna 2	φ_{A_2}	$-45°$
FMCW parameters		
Start frequency	f_start	77 GHz
Stop frequency	f_stop	79 GHz
Number of frequency points	N	512
SAR parameters		
Synthetic aperture length	L_x	0.06 m
Spatial sampling interval	Δu_x	1 mm
Number of spatial points	M_x	60

An accurate model of the measurement scenario is created by means of a field integral equation (IE) method which is solved numerically by the method of moments. To reduce the complexity of the numerical model, the IE approach is calculated for two dimensions at the center frequency of the sweep as explained in [1].

3. SIGNAL MODEL AND ALGORITHM

3.1. Data Preparation

This subsection explains the signal processing work-flow for estimating the position of the lap joint. Before x_K can be estimated, the measured data has to be preprocessed. In the measurements, the reference plane is located at the radio frequency chip on the frontend. For the simulations it is more convenient to have the reference plane in the aperture of the antennas. Thus, the electrical length of the conductors and the horn antenna can be interpreted as an additional phase shift between the measurement and the simulation reference plane. In order to have the same reference planes in the simulation and the measurement, the measured data are corrected accordingly. In the next step, the two-dimensional measured data set $X_{12}(k_\mathrm{r}, u_x)$ is reduced to one dimension. To this end, $X_{12}(k_\mathrm{r}, u_x)$ is Fourier transformed and scaled to range. The range bin $\hat{r}_\mathrm{max}$ is then computed by calculating $|X_{12}(r, u_x)|$ and summing it over all positions u_x. The bin containing the maximum of the sum corresponds to $\hat{r}_\mathrm{max}$, which corresponds to the dominant reflection of the lap joint. The data set is reduced by evaluating the data at the range bin $\hat{r}_\mathrm{max}$, which yields $X_{12,1\mathrm{D}}(u_x) = X_{12}(\hat{r}_\mathrm{max}, u_x)$. Fig. 2 shows the real and imaginary part of the one-dimensional measured data $X_{12,1\mathrm{D}}(u_x)$ and the simulation results $S_{12}(u_x)$ of a lap joint with a thickness of 10 mm normalized to the amplitude of the measured signal. Measurement and simulation are in very good agreement. The respective parameters are listed in Tab. 1. Reducing the measured data set to one dimension allows the IE approach to be calculated at one frequency, namely the center frequency of the radar sweep. Otherwise, the simulation would have to be performed for the whole frequency sweep, which would increase computational and memory effort.

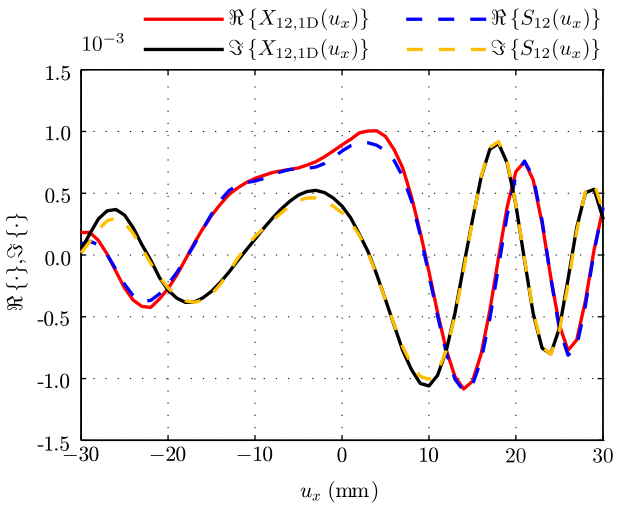

Fig. 2: Real and imaginary part of the measured data and the signal model for the parameter setup listed in Tab. 1.

3.2. Estimation

After data preprocessing, the signal $X_{12,1\mathrm{D}}(u_x)$ and the result from the numerical IE approach are used to estimate the position of the lap joint. Additionally, the thickness t of the top plate is assumed to be known. The data set is available on an equidistant grid at

$$u_x = m_x \Delta u_x \quad m_x = -\frac{M_x}{2}, -\frac{M_x}{2}+1, \ldots, \frac{M_x}{2}-1, \quad (2)$$

where Δu_x denotes the spatial sampling interval and M_x defines the number of spatial samples. The measurements are assumed to be corrupted with complex circular additive white Gaussian noise $w[m_x] \sim \mathcal{CN}(0, \sigma^2)$ with variance σ^2. Therefore, the measured data

$$X_{12,1\mathrm{D}}[m_x] = S_{12}[m_x] + w[m_x] \quad (3)$$

comprises a sum of the deterministic signal $S_{12}[m_x]$ and a stochastic part $w[m_x]$. The position of the lap joint is estimated by means of a maximum likelihood estimator (MLE). Thus, a reference signal $S_{12,\mathrm{ref}}[m_x] = S_{12}[m_x]|_{x_\mathrm{K}}$ is calculated for the known step thickness t with the numerical model. The cost function of the MLE can be written as

$$J = \sum_{m_x} \left| \left(X_{12,1\mathrm{D}}[m_x] - \tilde{A} S_{12,\mathrm{ref}}[m_x] \right) \right|^2, \quad (4)$$

where $\tilde{A}$ stands for the unknown complex amplitude. The complex amplitude is estimated by a separation approach

$$\tilde{A} = A e^{\mathrm{j}\phi} = \left(S_{12}^H[m_x]\big|_{\hat{x}_\mathrm{K}} \, S_{12}[m_x]|_{\hat{x}_\mathrm{K}} \right)^{-1} S_{12}^H[m_x]\big|_{\hat{x}_\mathrm{K}} \, X_{12,1\mathrm{D}}[m_x] \quad (5)$$

as described in [7, p. 194], where the superscript H denotes the Hermitian operator. The variable $S_{12}[m_x]|_{\hat{x}_\mathrm{K}}$ stands for the reference signal shifted to the estimated position $\hat{x}_\mathrm{K}$. Further, $\hat{(\cdot)}$ denotes that $\hat{x}_\mathrm{K}$ is an estimated parameter. The MLE for estimating the lap joint position

$$\hat{x}_\mathrm{K} = \arg\max_{x_\mathrm{K}} \left| \sum_{m_x} X_{12,1\mathrm{D}}[m_x] \left(S_{12,\mathrm{ref}}[m_x] \right)^* \right| \quad (6)$$

can be calculated efficiently in the spectral domain by using the shift property of the Fourier transform. This reduces the computational effort because the model has to be calculated with the IE only once. In this case, the MLE can also be interpreted in the context of a time delay estimation [7, p. 192] [8, p. 258] where the position shift $\hat{x}_\mathrm{K}$ (instead of the time delay) is estimated.

4. CRLB CALCULATION OF POSITION ESTIMATION

To assess the accuracy achieved, the CRLB (that is the minimum variance achievable) of the method is calculated. First, the elements of the Fisher information matrix [7, p. 49] are calculated, which - for a complex Gaussian probability density function - is given by

$$[\mathbf{I}(\theta)]_{ij} = \frac{2}{\sigma^2} \Re \left\{ \sum_{m_x=-\frac{M_x}{2}}^{\frac{M_x}{2}-1} \frac{\partial S_{12}^*[m_x,\theta]}{\partial \theta_i} \frac{\partial S_{12}[m_x,\theta]}{\partial \theta_j} \right\}. \quad (7)$$

In (7), $(\cdot)^*$ denotes complex conjugation. Here, θ is the vector of the unknown parameters

$$\theta = [x_\mathrm{K} \; A \; \phi]^T. \quad (8)$$

The variable x_K denotes the position of the lap joint, and $A > 0$ and $-\pi \leq \phi < \pi$ are the amplitude and the phase of the measured signal, respectively. The superscript T describes a matrix transposition. The signal model $S_{12}[m_x]$ is obtained from a numerical field simulation and not known analytically. Therefore, the derivation in (7) is approximated by the central difference quotient according to

$$\frac{\partial S_{12}[m_x,\theta]}{\partial \theta} \approx \frac{S_{12}[m_x,\theta+\Delta\theta] - S_{12}[m_x,\theta-\Delta\theta]}{2\Delta\theta}. \quad (9)$$

The main diagonal elements of $\mathbf{I}^{-1}$ are the best achievable variances of the corresponding parameter estimation, assuming an unbiased estimator. Therefore, the minimum position variance achievable is calculated by

$$\mathrm{var}\{\hat{x}_\mathrm{K}\} \geq \left[I(\theta)^{-1} \right]_{11}. \quad (10)$$

5. MEASUREMENT AND SIMULATION RESULTS

5.1. Monte Carlo Simulation

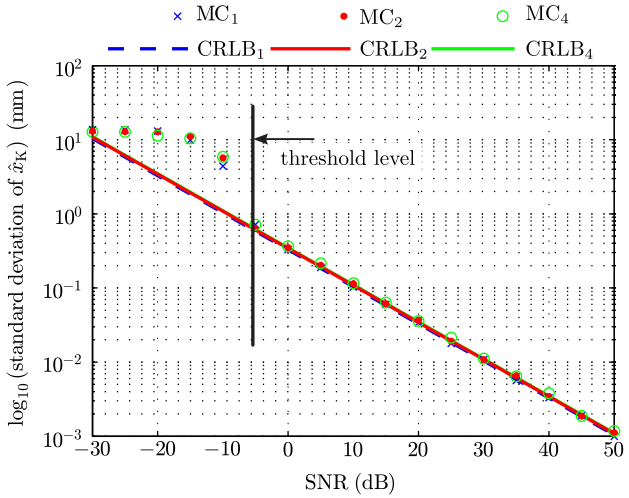

Fig. 3: Standard deviations of the position estimations for thicknesses $t = \{1, 2, 4\}$ mm compared to MC simulation results.

MC simulations were carried out to verify the CRLB introduced in Section 4. The parameters of the calculations are

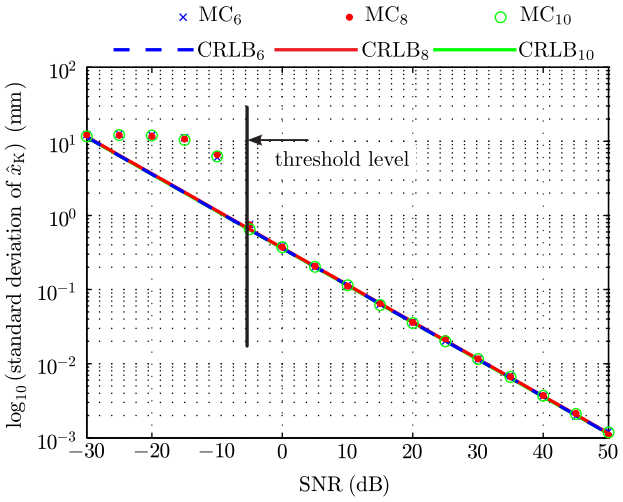

Fig. 4: Standard deviations of the position estimations for thicknesses $t = \{6, 8, 10\}$ mm compared to MC simulation results.

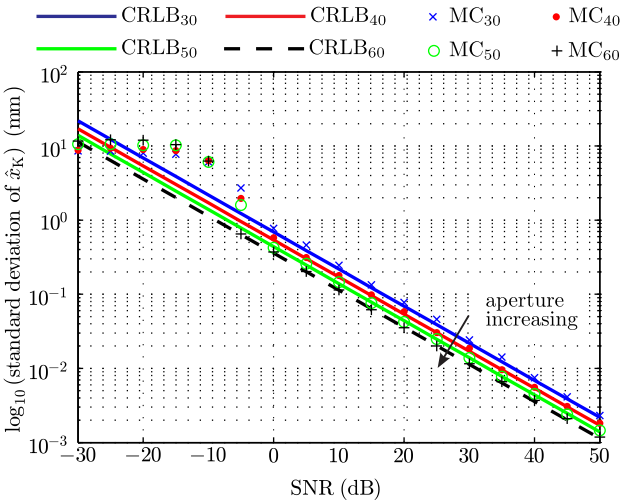

Fig. 5: Standard deviations of the position estimations for different synthetic apertures $L = \{30, 40, 50, 60\}$ mm compared to MC simulation results.

summarized in Tab. 1. Additionally, the thickness of the lap joint was varied for $t = \{1, 2, 4, 6, 8, 10\}$ mm. Furthermore, the influence on the CRLB, depending on different aperture widths L and different spatial sampling intervals Δu_x were investigated and are reported here. All results were verified with MC simulations for different σ^2, and 500 realizations for each noise level were performed to validate the algorithm. Since the variance of the position estimation varies with the noise power, the signal-to-noise ratio (SNR) of our signal had to be calculated. The SNR is defined as

$$\mathrm{SNR} = \frac{P_{\mathrm{sig}}}{\sigma^2}. \tag{11}$$

The variable P_{sig} is the signal power, which is defined as

$$P_{\mathrm{sig}} = \frac{1}{L} \int_{-\frac{L}{2}}^{\frac{L}{2}} S_{12}(u_x) S_{12}^*(u_x) \mathrm{d}u_x. \tag{12}$$

Fig. 3 shows the standard deviation $\sigma_{\hat{x}_\mathrm{K}} = \sqrt{\mathrm{var}\left(\hat{x}_\mathrm{K}\right)}$ of the CRLB calculation and the results of the MC simulation for $t = \{1, 2, 4\}$ mm (CRLB_t, MC_t). Fig. 4 plots the results for $t = \{6, 8, 10\}$ mm. Both figures show that the position estimation algorithm practically reaches the CRLB. Further, the standard deviation is independent of the lap joint thickness t. The lap joint position can be estimated with a standard deviation in the sub-millimeter region. The threshold level can be identified at an SNR of -6 dB. The threshold effect occurs below a certain level of SNR where the performance of the estimator significantly deviates from the CRLB. When the SNR level is low, local minima lower than the global minimum and local maxima higher than the global maximum can appear in the cost function. Hence, the optimization process chooses the wrong maximum, which results in the threshold [9, 10]. For future investigations the threshold behavior can be calculated to determine the exact SNR limit.

Fig. 5 illustrates the effect of different aperture widths on the CRLB. In the calculations, the number of spatial sampling points was constant ($M_x = 60$), and the synthetic aperture was swept from $L = \{30, 40, 50, 60\}$ mm (CRLB_L, MC_L). All calculations were verified with MC simulations. The figure clearly shows that the variance increases when shrinking the synthetic aperture. However, the standard deviation of the position estimation, even for the shortest aperture $L = 30$ mm, remains very low.

In the last simulation, the synthetic aperture was kept constant at $L = 60$ mm, and the number of spatial sampling points was swept from $M_x = \{60, 120, 240, 480\}$ (CRLB_{M_x}, MC_{M_x}). Fig. 6 plots the results of the calculations and MC simulations, which clearly show that increasing the number of spatial sampling points decreases the variance of the estimator.

5.2. Verification of CRLB

To verify the simulation results presented in Section 5.1 measurements with a lap joint of 10 mm thickness were conducted. To this end, a vector network analyzer (VNA) working at a center frequency of $f_c = 27.5$ GHz with a frequency bandwidth $B = 2$ GHz was used as a radar system. A 27.5 GHz hardware was used in place of the obviously preferable 77 GHz VNA for reasons of availability. A synthetic aperture of $L = 0.1$ m with a spatial sampling interval $\Delta u_x = 2$ mm was performed. Each reported measurement at each aperture point is based on 500 individual trials and different SNR values, which were generated by sweeping the output power of the VNA. Subsequently, the measured data was reduced to one dimension as described in Section 3.1. Prior to calculating the variance of the position estimation the SNR had to be estimated. The noise power $\hat{\sigma}^2$ was estimated in the spectral domain as described in [7]. Then, the signal power $\hat{P}_{\mathrm{sig}}$ is computed by calculating the total power P_{tot}

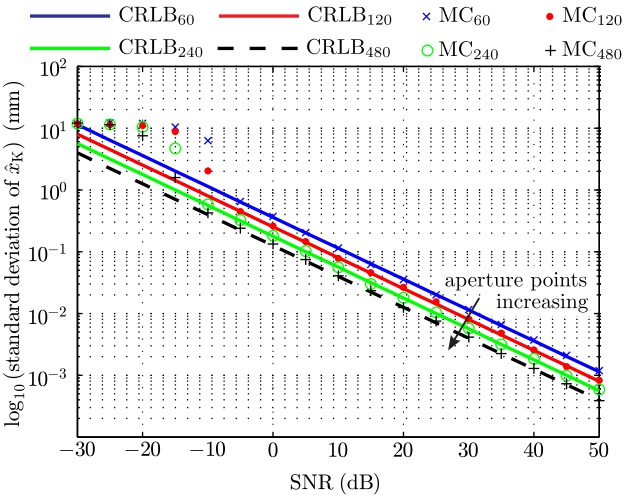

Fig. 6: Standard deviations of the position estimations for different spatial sampling points $M_x = \{60, 120, 240, 480\}$ compared to MC simulation results.

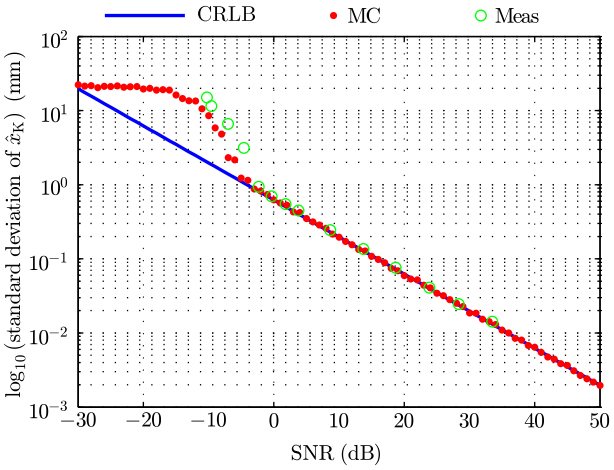

Fig. 7: Standard deviation of the position estimation. The calculated CRLB is verified by an MC simulation and measurements.

and subtracting the noise power.

$$\hat{P}_{\text{sig}} = \underbrace{\frac{1}{L}\int_{-\frac{L}{2}}^{\frac{L}{2}} X_{12}(u_x)X_{12}^{*}(u_x)\mathrm{d}u_x}_{P_{\text{tot}}} - \hat{\sigma}^2. \qquad (13)$$

Subsequently, the position estimation was carried out for all trials and SNR levels. Fig. 7 shows the resulting standard deviations based on the measurements and an MC simulation. Additionally, the calculated CRLB is shown. The calculation, the measurement, and the simulation results are in very good agreement, which validates the calculated bound.

6. CONCLUSION

In this paper, the CRLB for a novel position estimation approach based on polarimetric scattering effects was calculated and validated by MC simulations and measurements. The results show that the CRLBs derived hold for the position estimation for the setups investigated. Our discussions and simulations examined various influences on the achievable variance and can be used to design FMCW radar-based measurement scenarios for high-accuracy applications.

7. ACKNOWLEDGMENT

This work was funded by the COMET/K-project JOIN4+ (825318).

8. REFERENCES

[1] J. Schrattenecker, A. Haderer, G. Reinthaler, and A. Stelzer, "Position Estimation of Lap Joints for Seam Tracking Applicaitons at mm-Wave Frequencies," *Radar Conference (EuRAD)*, pp. 71–74, 2012.

[2] A. Haderer, P. Scherz, and A. Stelzer, "Position Estimation of Thin, Conducting Plates at mm-Wave Frequencies Utilizing Polarimetric Effects," *IEEE MTT-S Int. Microw. Symp. Dig. 2011*, 2011.

[3] Constantine A. Balanis, *Advanced Engineering Electromagnetics*, John Wiley & Sons, Inc., New York, 1989.

[4] A. G. Stove, "Linear FMCW Radar Techniques," *IEE Proc. F, Radar Signal Processing*, vol. 139, no. 5, pp. 343–350, Oct. 1992.

[5] Mehrdad Soumekh, *Synthetic Aperture Radar Signal Processing with MATLAB Algorithms*, John Wiley & Sons, Inc., New York, 1999.

[6] I. G. Cumming and F. H. Wong, *Digital Processing of Synthetic Aperture Radar Data: Algorithms and Implementation*, Artech House, Boston, 2005.

[7] S. M. Kay, *Fundamentals of Statistical Signal Processing: Estimation Theory*, Prentice Hall PTR, Upper Saddle River and NJ, 1993.

[8] S. M. Kay, *Fundamentals of Statistical Signal Processing: Detection Theory*, Prentice Hall PTR, Upper Saddle River and NJ, 1998.

[9] B. G. Quinn and P. J. Kootsookos, "Threshold Behavior of the Maximum Likelihood Estimator of Frequency," *IEEE Trans. Signal Proc.*, vol. 42, no. 11, pp. 3291–3294, Nov. 1994.

[10] Harry L. van Trees, *Detection, Estimation, and Modulation Theory - Part l - Detection, Estimation, and Linear Modulation Theory*, John Wiley & Sons, Inc., Hoboken, 2001.